Polymer 229 (2021) 123966

Contents lists available at ScienceDirect

Polymer

journal homepage: www.elsevier.com/locate/polymer

Influence of loading conditions on the tensile response of degraded polyamide 11

Sindre Nordmark Olufsen [a,*], Per Nygård [b], Catarina Ines Teixeira Pais [b], Giovanni Perillo [b], Odd Sture Hopperstad [a], Arild Holm Clausen [a]

[a] Centre of Advanced Structural Analysis (SFI CASA), Department of Structural Engineering, Norwegian University of Science and Technology (NTNU), NO-7491, Trondheim, Norway
[b] Equinor Research and Technology, NO-7053, Trondheim, Norway

ARTICLE INFO

Keywords:
Mechanical testing
Polyamide 11
Degradation
Embrittlement
Digital image correlation

ABSTRACT

The chemically induced embrittlement of polyamide 11 (PA11) has been the subject of a considerable research effort to understand and predict the degree of embrittlement based on the material's intrinsics. However, the presence of highly complex loading scenarios and stress states in real-world structures raises the question of whether extrinsic factors such as loading conditions and temperature also affect the mechanical response of the degraded material. Motivated by this, this study investigates how the large-strain tensile response of chemically degraded PA11 is influenced by temperature, strain rate and stress triaxiality. Material samples with plasticizer contents of 0% and 6% were chemically degraded by exposure to butanoic acid at elevated temperature. The mechanical properties were determined by tensile testing of round notched samples while measuring local strains using digital image correlation. The mechanical responses span from highly ductile behaviour with necking and subsequent cold-drawing to a brittle response without any apparent plasticity. Reduced ductility was found for increasing degradation, amplified when the temperature, the notch radius or the softener content was reduced. A comparison of local and nominal strains showed that large local strains could be present even on samples which appear brittle when only nominal strains are measured. This study demonstrates that both a brittle and a ductile response can be obtained for the same state of chemical degradation by varying the loading conditions.

1. Introduction

Polyamide 11 (PA11) is a semi-crystalline polymer extensively used in a wide range of applications, spanning from sports equipment to oil pipelines. Due to its comparatively good chemical resistance and high ductility, PA11 has been extensively used by the petroleum industry. However, reduced ductility has been reported due to long term exposure to corrosive environments, triggering an extensive research effort assessing the embrittlement of PA11. Degradation due to oxidation, hydrolysis and exposure to an acidic environment has been observed, reducing the ductility of the material [1,2].

In order to ensure safe operation of structures made of PA11, a metric describing the degree of embrittlement has been sought after. Field experience and laboratory studies on the degradation of PA11 have shown that the molecular weight decreases and the degree of crystallinity increases during degradation, leading to an abrupt reduction in ductility. Motivated by this observation, a critical molecular weight has been extensively used as an indicator of the degree of embrittlement. In practical applications, the average molecular weight is often reported as the corrected inherent viscosity (CIV), a metric also used in API TR 17TR2 [3].

However, significant differences in elongation at failure have been reported for similar molecular weights [4], suggesting that CIV alone is not a reliable predictor of the degree of embrittlement. During degradation, the increased mobility of the shorter molecular chains promotes a process commonly referred to as chemi-crystallization [1,4,5], which increases the degree of crystallinity. Simultaneously, the thickness of the amorphous layer in the semi-crystalline material decreases [1,4,5]. Therefore, the degree of crystallinity, or more precisely, the average thickness of the amorphous layers, has been proposed as an alternative metric for predicting the degree of embrittlement in degraded PA11 [1,4].

A concern in the assessment of load bearing structures made of degraded PA11 is the complex load cases associated with real-world

* Corresponding author.
E-mail address: sindre.n.olufsen@ntnu.no (S.N. Olufsen).

https://doi.org/10.1016/j.polymer.2021.123966
Received 21 May 2021; Received in revised form 23 June 2021; Accepted 23 June 2021
Available online 30 June 2021
0032-3861/© 2021 The Authors. Published by Elsevier Ltd. This is an open access article under the CC BY license (http://creativecommons.org/licenses/by/4.0/).

applications. This raises the question whether the transition from a ductile response to a brittle response could be coupled not only to the intrinsics of the material represented by the CIV or amorphous layer thickness but also to the load case and temperature. The tensile response of thermoplastics is typically affected by strain rate [6], stress triaxiality [7,8] and temperature [1,6], factors which possibly could influence the transition towards a more brittle response.

As the degradation process affects the microstructure of the material, several characteristics of the mechanical response are anticipated to change during degradation. During the deformation of semi-crystalline polymers, a complex interplay between the amorphous and semi-crystalline phase is observed [9–11]. The amorphous phase, being the phase where the chain scission process is anticipated to be most prominent, has a strong influence on the mechanical behaviour of semi-crystalline polymers, including the elastic properties, rate-sensitivity, hardening and locking behaviour, and thereby the ductility in general [12,13].

Another factor influencing the response of the material is the presence of plasticizers, also referred to as softeners. Plasticizers are commonly added to semi-crystalline polymers during production to moderate the degree of crystallinity, improve the manufacturability and reduce the glass transition temperature. A commonly used plasticizer for PA11 is N-Butylbenzenesulfonamide (BBSA). However, experience from the petroleum industry has shown that the plasticizer content of the material may decrease after long term use, questioning whether the decreased plasticizer contents affect the response of the degraded material.

When designing an experimental campaign to investigate how chemical degradation influences the tensile properties of a polymeric material, selecting the appropriate experimental conditions is a key issue. By increasing the strain rate or decreasing the temperature of the specimen, the stress level is increased [1,6]. By employing notched tensile specimens, a triaxial stress state is obtained in the notch region of the specimen, which has been shown to promote void growth in thermoplastics such as PVC [7,8,14], PA6 [15] and PA11 [16].

Traditionally, strains have been measured by a mechanical extensometer attached to the surface of the tensile specimen or by using the displacement of the test apparatus. In both cases, homogeneous deformation is assumed. However, polymeric materials often have limited strain hardening, and in some cases even strain softening, promoting the formation of a neck on the tensile specimen at a comparatively early deformation stage. After a neck has formed, accurate strain measurements are only feasible using full-field measurements techniques such as digital image correlation (DIC). Also, local strain measurements allow for calculation of the true stress-strain curve and estimation of the volumetric strain. When volumetric strains are estimated from measurements of the deformation on the surface, the inherent assumption used in such calculations introduces errors [14,17].

In this study, we investigate the influence of temperature, strain rate and stress triaxiality on the tensile response of PA11 with two plasticizer contents degraded to two CIV levels. Motivated by the high degradation rates reported by Hocker et al. [4], the PA11 material was degraded using a water-butanoic-acid solution in an autoclave at elevated temperature. Axisymmetric notched tensile specimens are used, allowing for varying the initial stress triaxiality ratio. All tests are instrumented with two digital cameras, allowing the local strain within the notch region to be determined by DIC. Due to the numbers of parameters, a two-factor experimental design was employed for identification of the parameters with the largest impact on the tensile response of the material, thereby disclosing the experimental conditions that lead to a more brittle behaviour of degraded PA11.

2. Experimental

2.1. Experimental design

A two-level factorial design is used to gain an understanding of the main effects and interactions of temperature, strain rate, stress triaxiality ratio, CIV-level and plasticizer on the tensile response of PA 11. The levels of the five selected factors are summarised below:

- Temperature: 10 °C and 23 °C
- Nominal strain rate: 10^{-3} s^{-1} and 10^{-1} s^{-1}
- Notch radius: 2 mm and 20 mm
- CIV levels: 0.7 dL/g and 1.2 dL/g
- Initial plasticizer content: 0% and 6%

The high and low levels of the five factors were chosen such that they have a span relevant for the assessment of offshore pipelines. The lower bound of the temperature range was motivated by the anticipated temperature during gas expansion in oil and gas pipelines, whereas the upper bound was chosen to lie between the glass transition temperature of the two investigated PA11 grades. Both strain rates are considered as quasi-static from an experimental point of view, while the higher one of 10^{-1} s^{-1} approaches a level that is relevant for assessment of dynamic structures. The two notch radii of 20 mm and 2 mm correspond respectively to an initial stress triaxiality ratio in the centre of the notch of 0.4 and 0.8. Thus, the initial stress triaxiality ratios span from nearly uniaxial tension to a moderately high triaxiality [8]. The CIV levels were chosen such that the upper value of 1.2 dL/g is in the order of the lowest recommended CIV for safe use in offshore pipeline applications according to API TR 17TR2 [3], and the lowest value represents a heavily degraded material, anticipated to have a brittle response. The plasticizer contents represent two stages of plasticizer wash-out, the upper level being 6% and the lower level of 0% represents material where the plasticizer has vanished completely. It should be noted here that the commercial PA11 material used in offshore pipeline applications has an initial plasticizer content of 12%.

As five factors are investigated at two levels, $2^5 = 32$ unique experiments were performed. Due to practical constraints in the experimental setup, the order of the experiments was not randomised completely.

To get an indication of the repeatability of the experiments, two replicate tests were carried out for the four factor combinations expected to be most critical. The high-triaxiality specimens with a CIV of 0.7 dL/g and 0% softener were likely to be most brittle, and were selected for replicate testing. The repeat tests were performed for all four combinations of strain rates and temperatures on these specimens, raising the total number of tests to 36.

2.2. Material degradation and analysis

The investigated material is RILSAN™ Polyamide 11 provided by Arkema. Two purpose-made batches of plates with thickness 10 mm were produced with a N-Butylbenzenesulfonamide (BBSA) plasticizer content of 6% and 0%. The producer reported that the glass transition temperature was around 50 °C for the material with 0% softener and 0 °C for a softener content of 6%.

Motivated by the rapid degradation rates reported by Hocker et al. [2], a 6.6×10^{-2} M solution of butanoic acid in deionized water was used to chemically degrade the material by reducing the average molecular weight. PA11 samples and 2.0 L of the solution were placed in a 2.5 L autoclave and the liquid phase was bubbled with nitrogen for 3 h to remove oxygen and thereby prevent oxidative degradation of the samples. The autoclave was then pressurised with nitrogen to 0.5 bar and the temperature was set to 120 °C. In order to counteract the extraction of softener from the material during degradation, BBSA was added to the solution for the specimens with a softener content of 6%. When

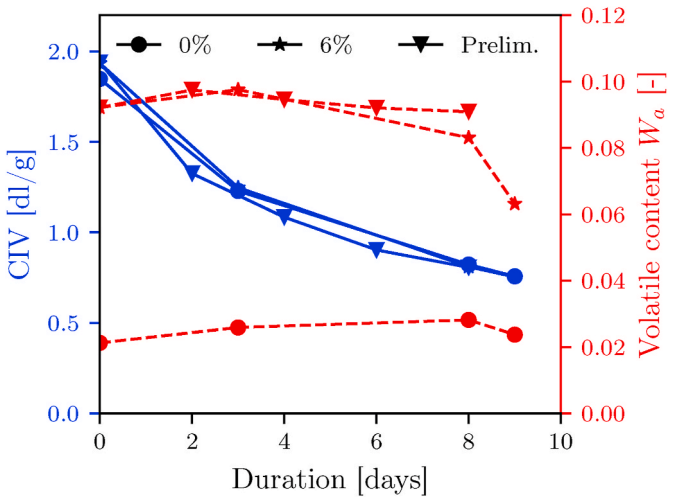

Fig. 1. Measurements of CIV (blue) and weight fraction W_a of volatile content (red) for different durations in the autoclave for dummy samples with a plasticizer content of 0% and 6%. Results from the preliminary experiment (Prelim.) are also included. The points represent the average values of the measurements at two depths within the sample being 0–900 μm and 900–1800 μm.. (For interpretation of the references to colour in this figure legend, the reader is referred to the Web version of this article.)

specimens were retrieved from the autoclave, the oxygen removal procedure was repeated and the pH was measured. The butanoic acid solution had a constant pH of approximately 3 throughout the whole degradation process.

In order to determine the degradation time necessary to reach a given CIV, a preliminary degradation experiment was performed using low-cost dummy samples. Dummy samples with a plasticizer content of 6% and a thickness of 6 mm were employed, and the evolution of CIV was measured at given time intervals during degradation. These dummy samples had rectangular cross section with similar dimensions as the axisymmetric tensile specimen presented in Section 2.3. The samples were retrieved from the autoclave after 2, 4, 6 and 8 days. Applying the procedure to be described shortly, the CIV values of these samples were measured near the surface and in the interior of the samples. This preliminary analysis suggested that the tensile specimens should be exposed to the degradation procedure for 3 and 9 days to reach the target CIV values of 1.2 dL/g and 0.7 dL/g, respectively.

The degradation of the tensile specimens was performed in two separate autoclaves, one for each plasticizer content. In order to monitor the CIV during the degradation procedure, 6 mm thick dummy samples were also included in the autoclaves along with the tensile specimens. Samples were retrieved after 3, 8 (verification only) and 9 days. During the degradation process, the corrected inherent viscosity (CIV) and the volatile content, i.e. the weight fraction W_a of additives, were measured on the dummy specimens included in the autoclave. The measurements were carried out in two layers of each dummy sample; one layer within 900 μm from the surface, and one layer between 900 and 1800 μm from the surface.

The corrected inherent viscosity was determined by a method based on API TR 17TR2 [3]. First, the inherent viscosity IV of a PA11:*m*-cresol solution was measured with an Ubbelohde viscometer at 20 °C. The inherent viscosity is defined as:

$$\mathrm{IV} = \frac{\ln(t/t_0)}{c} \tag{1}$$

where t is the flow time for the solution and t_0 is the flow time for *m*-cresol, and c is the concentration in g/dL. The viscosity of a polymer solution is affected by the presence of additives, such as plasticizers and absorbed water, and the inherent viscosity needs to be corrected to account for the additives present in commercial polyamide grades. The corrected inherent viscosity CIV is calculated as:

$$\mathrm{CIV} = \frac{\mathrm{IV}}{1 - W_a} \tag{2}$$

where IV is given in dL/g. The weight fraction W_a of additives, or the volatile content, was measured by thermogravimetric analysis (TGA) using a Mettler Toledo TGA/DSC 1 apparatus. Further description on the procedure used to calculate the CIV is found in API TR 17TR2 [3]. Samples taken from the specimens were heated from 25 °C to 200 °C at 40 °C min^{-1}, and held at 200 °C for 150 min under a helium gas flow of 40 mL/min. The un-aged samples were submerged in water at room temperature prior to the TGA measurements.

The results from the measurement of CIV and volatile content from both degradation experiments are shown in Fig. 1. The numerical values are compiled in Table 1 and Table 2. It appears from the tables that there are only minor differences between the CIV and volatile content in the two investigated layers of the dummy specimens.

The degree of crystallinity χ_c was determined by differential scanning calorimetry (DSC) [18] for a small piece of material cut from a tensile specimen using an Mettler Toledo DSC 1 instrument. Approximately 6 mg of sample was weighed into a 40 μL aluminium crucible with pierced lid and crimp sealed. The samples were analysed in an inert atmosphere, with a constant nitrogen flow of 40 mL/min, and the following temperature sequence:

1. Cool to −40 °C at 50 °C min^{-1}
2. Hold at −40 °C for 10 min
3. Heat from −40 °C to 220 °C at 20 °C min^{-1}

Table 1
Results from the preliminary degradation experiment showing corrected inherent viscosity (CIV) and weight fraction of volatile content (W_a) measured on dummy samples for four durations in the autoclave. The measurements are performed at two depths within the sample being 0–900 μm (out.) and 900–1800 μm (in.).

Days	Depth	CIV [dL/g]	W_a[−]
0	out.	1.95	0.0931
0	in.	1.93	0.0913
2	out.	1.27	0.1010
2	in.	1.39	0.0938
4	out.	1.04	0.0943
4	in.	1.13	0.0949
6	out.	0.87	0.0940
6	in.	0.93	0.0901
8	out.	0.78	0.0940
8	in.	0.83	0.0978

Table 2
Results from the degradation of tensile specimens showing corrected inherent viscosity (CIV), weight fraction of volatile content (W_a) and crystallinity (χ_c) for three durations in the autoclave. The measurements of CIV and W_a are performed at two depths within the sample being 0-900 μm (out.) and 900-1800 μm (in.).

Days	Depth.	0% softener			6% softener		
		CIV [dL/g]	W_a[−]	χ_c [%]	CIV [dL/g]	W_a[−]	χ_c [%]
0	out.	1.83	0.0217		1.94	0.0930	
0	in.	1.86	0.0208		1.93	0.0913	
3	out.	1.16	0.0266	28[a]	1.19	0.0995	29[a]
3	in.	1.30	0.0253	28[a]	1.30	0.0956	29[a]
8	out.	0.79	0.0307		0.78	0.0842	
8	in.	0.86	0.0257		0.84	0.0820	
9	out.	0.72	0.0237	32[a]	0.74	0.0657	34[a]
9	in.	0.79	0.0238	32[a]	0.77	0.0606	34[a]

[a] This measurement was performed on a single piece of material collected from a tensile specimen.

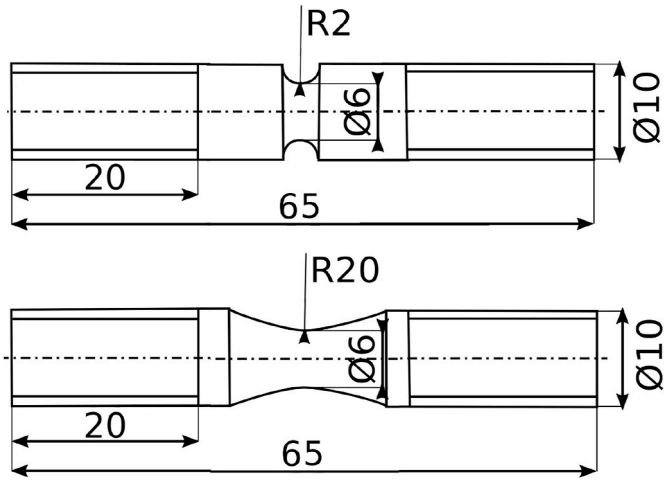

Fig. 2. Schematic of the axisymmetric notched tensile specimens. Dimensions are given in mm.

4. Hold at 220 °C for 1 min
5. Cool from 220 °C to −40 °C at 20 °C min^{-1}
6. Hold at −40 °C for 10 min
7. Heat from −40 °C to 220 °C at 20 °C min^{-1}

The degree of crystallinity (in %) was calculated as:

$$\chi_c = \frac{\Delta H_f}{\Delta H_f^0 (1 - W_a)} \times 100 \tag{3}$$

where $\Delta H_f^0 = 225$ Jg^{-1} is the melting enthalpy for 100% crystalline PA11 reported by Arkema and ΔH_f is the specific enthalpy of fusion, determined as the area under the melting peak in the first heating. The crystallinity was corrected to account for the weight fraction of additives, W_a, determined by TGA. The results from the DSC analysis are compiled in Table 2, showing that χ_c increases with increasing degradation.

The CIV and volatile content measured on the dummy samples reveal minor gradients in both metrics in the outer 2 mm of the samples, see Tables 1 and 2 As the stress and strain fields are inhomogenous within the notched section of the samples, a gradient in the material properties could influence the tensile response of the specimens, but the magnitude is not assessed in this study. For increasing degradation, the volatile content shows a non-linear evolution for the specimens with 0% softener, peaking at eight days, while the volatile content at 3 and 9 days is similar. Despite the addition of BBSA to the autoclave for the specimens with an initial softener content of 6%, a reduced volatile content is observed for the samples extracted after 9 days, making the softener content dependent on the CIV level for these specimens.

2.3. Mechanical testing

Axisymmetric notched tensile specimens were applied to vary the initial stress triaxiality ratio in the notch. Notch radii of 2 mm and 20 mm were used, giving an initial stress triaxiality ratio in the centre of the notch of 0.8 and 0.4, respectively [8]. A schematic of the tensile specimens is shown in Fig. 2. Note that during deformation, the stress triaxiality ratio will change both due to geometric changes and due to deformation-induced cavitation (if present).

The specimens were produced from the two batches of PA11 plates with softener contents of 0% and 6%. A total of 36 specimens were produced, 32 represents different factor combinations and four being selected duplicates of four of the factor combinations. After machining, the specimens were chemically degraded using the procedure described in Section 2.2. All tensile specimens that were retrieved from the autoclaves were slightly curved with a typical deflection of 2 mm. As this study pays attention to ductility and the response at large deformations, this minor initial curvature is not believed to impose any significant source of error.

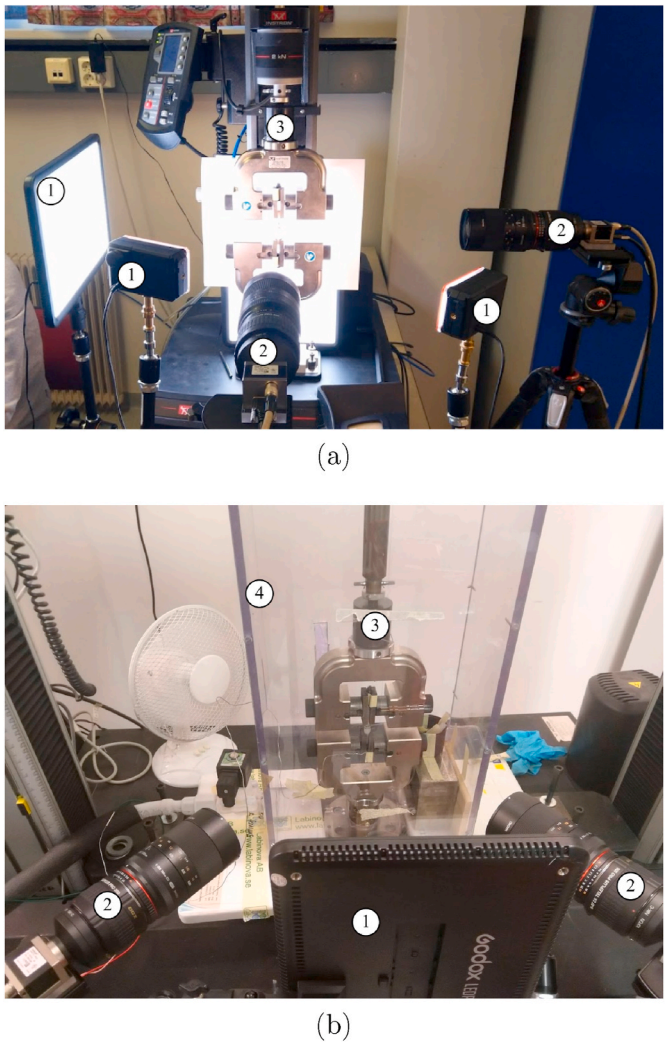

Fig. 3. Experimental setup used for tensile test at a) 23 °C and b) at −10 °C, with lighting (1), cameras (2), tensile test apparatus (3) and transparent cooling chamber (4).

An airbrush and black paint was used to apply a speckle-like pattern to the specimens tested at room temperature to facilitate digital image correlation. In order to avoid cracking of the speckle at low temperature, grease and black powder were used to produce a speckle on the surface of specimens tested at −10 °C. A similar approach was applied by Johnsen et al. [19].

Fixation of the tensile specimens to the tensile test apparatus was facilitated by threading both ends of the specimens. However, due to problems with premature failure of the threads during testing, clamps were used in the experiments.

The tensile tests were performed at two different temperatures, being room temperature (23 °C) and low temperature (−10 °C). Tensile testing at room temperature was performed by an Instron 5940 test machine, whereas an Instron 5566 test machine was used in the low-temperature tests. The tensile test machines were equipped with a 2 kN and a 10 kN load cell, respectively. The experimental setups are shown in Fig. 3. Targeting an initial strain rate in the order of 10^{-1} s^{-1}, the piston speed of the tensile test apparatus was set to 0.4 mm/s and 0.53 mm/s for the R2 and R20 specimens, respectively. For the samples targeting an initial

strain rate in the order of $10^{-3}\,s^{-1}$, the applied speeds were reduced by a factor of 100.

A transparent temperature-controlled chamber developed by Johnsen et al. [19], allowing for instrumentation with digital cameras, was used for the tensile tests at low temperature. A stable temperature of $-10\,^{\circ}C$ inside the chamber was obtained by injecting liquid nitrogen at a rate governed by a temperature sensor and a PID-controller. This injection process was in operation during testing of the specimens deformed at low rate. In order to avoid haze effects when liquid nitrogen was injected into the chamber, the injection was disabled immediately before testing of the specimens deformed at high rate. To ensure that thermal equilibrium was reached before tensile testing, the specimens tested at low temperature were cooled in the low-temperature chamber for 1 h and subsequently clamped in the tensile test apparatus. The time used for cooling the samples was motivated by simulations performed by Ilseng et al. [20,21]. Applying the same cooling chamber with a target temperature of $-18\,^{\circ}C$, they concluded that 8 min was sufficient for preconditioning their samples made of a material with 2 mm thickness and approximately twice the thermal conductivity. It should also be noted that the simulations performed by Ilseng et al. [20,21] assumed natural convection in contrast to the forced convection enforced by the gas injection in the thermal chamber, making the simulated cooling rate a conservative estimate. After the specimen was clamped in the tensile test apparatus, the temperature of the specimen was stabilised for another 10 min before the tensile test was initiated.

Images for digital image correlation were captured by two orthogonally positioned 12 MP Basler AC4112-30UM cameras equipped with Samyang f/2.8 ED UMC lenses with a focal length of 100 mm at an aperture of F/12. In order to minimise the distortion of the lenses and spurious strains [22], teleconverters were used to increase the effective focal length of the lenses to 200 mm. The distance between the lens and the tensile specimen was approximately 300 mm in all tests. During tensile testing, the acquisition rate was limited by the exposure time of the cameras and between 50 and 200 images were captured for the specimens tested at high rate. For the specimens tested at low rate, between 500 and 2000 images were acquired during each test.

Force and displacement were measured by the tensile test machine and combined with the surface strain measurements acquired by DIC to calculate the true longitudinal strain ϵ_l and the true radial strain ϵ_r. Close correspondence was observed for the strain measurements from the two orthogonal cameras, and the average value is therefore reported as the true strain hereafter. The DIC analysis was performed by two in-house DIC codes named eCorr [23] and μDIC [24]. eCorr allows for grey scale normalisation, being necessary to account for haze effects observed in some of the image series acquired at the lowest strain rate, whereas μDIC allows for batch analysis. The procedure used to determine the longitudinal and radial strains from the measurements is described by Olufsen et al. [7].

The true stress σ was determined as:

$$\sigma = \frac{F}{A_0 \lambda_r^2} \tag{4}$$

where F is the force measured by the tensile test apparatus, A_0 is the area of the minimum cross-section of the notch before deformation and $\lambda_r = e^{\epsilon_r}$ is the radial stretch. The DIC measurements of λ_r were verified by measurements obtained by an edge tracing routine.

Cavitation is assessed by monitoring the volumetric strain evolution during the tensile test. The average volumetric strain of a disc spanning the minimum cross-section of the notch is calculated as [7]:

$$\epsilon_v = \ln(\lambda_l \lambda_r^2) \tag{5}$$

where $\lambda_l = e^{\epsilon_l}$ is the longitudinal stretch as measured by DIC. It should be noted that due to the inherent assumption used in the calculation of volumetric strain from DIC measurements, the accuracy of the estimates is questionable [14,17]. However, as the estimates are interpreted in a qualitative manner only, the accuracy of the estimates is considered satisfactory for the purpose of this study.

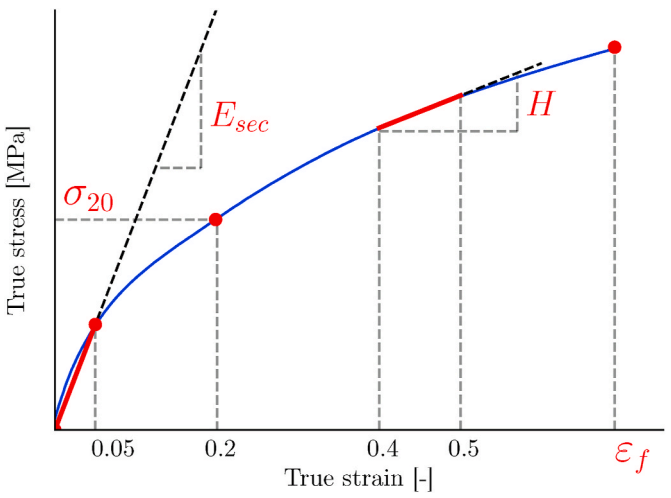

Fig. 4. True stress-strain curve (blue) shown together with the segments used to calculate the response parameters (red). (For interpretation of the references to colour in this figure legend, the reader is referred to the Web version of this article.)

2.4. Factor analysis

To aid the interpretation of the results from the tensile tests, the methodology presented by Montgomery [25] is used to calculate the main effects and interactions of temperature, rate, notch radius, CIV and initial softener content on selected response parameters. The following response parameters are extracted from each experiment:

- Secant modulus E_{sec}
- Yield stress σ_{20}
- Hardening modulus H
- True strain at failure ϵ_f

The response parameters are shown on a generic true stress-strain curve in Fig. 4.

The secant modulus E_{sec} is calculated as the secant of the true stress-strain curve between true strains of 0 and 0.05, and is used as a measure of the initial stiffness of the material. The yield stress σ_{20} is here defined as the true stress at a true strain of 0.2, corresponding to 20%. Further, the hardening modulus H is determined as the secant of the true stress-strain curves between true strains of 0.4 and 0.5. The true strain at failure ϵ_f is extracted when visual surface cracks are formed or the mesh used in the DIC analysis moves out of the image.

The main effect A of changing a variable a from its low level to its high level, all other variables held constant, is calculated as:

$$A = \bar{y}_{a^+} - \bar{y}_{a^-} \tag{6}$$

where $\bar{y}_{a^+}$ and $\bar{y}_{a^-}$ denotes the average value of the response parameter y when the variable a is in its high and low level, respectively. In a similar manner, the interaction AB between the variables a and b can be calculated as the effect of changing the variable a at the two levels of the variable b:

$$AB = \frac{(\bar{y}_{a^+b^+} - \bar{y}_{a^-b^+}) - (\bar{y}_{a^+b^-} - \bar{y}_{a^-b^-})}{2} \tag{7}$$

where $\bar{y}_{a^+b^+}$ and $\bar{y}_{a^-b^+}$ denotes the average value of the response parameter y when the variable a is in its high and low level respectively,

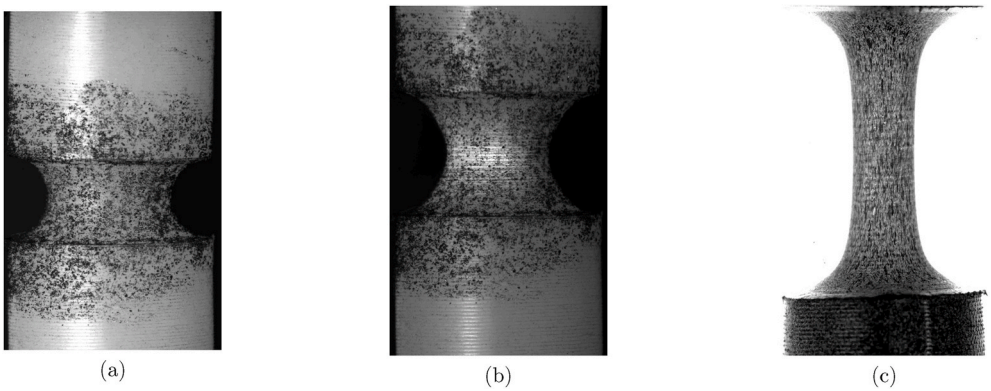

Fig. 5. Comparison of deformed shapes immediately before failure of (a) a brittle specimen, (b) a specimen that fails at necking, and (c) a specimen that fails after cold drawing. Note that the brittle specimen failed in the vicinity of the threads. Note the formation of horizontal cracks on the specimen surface in figure (b).

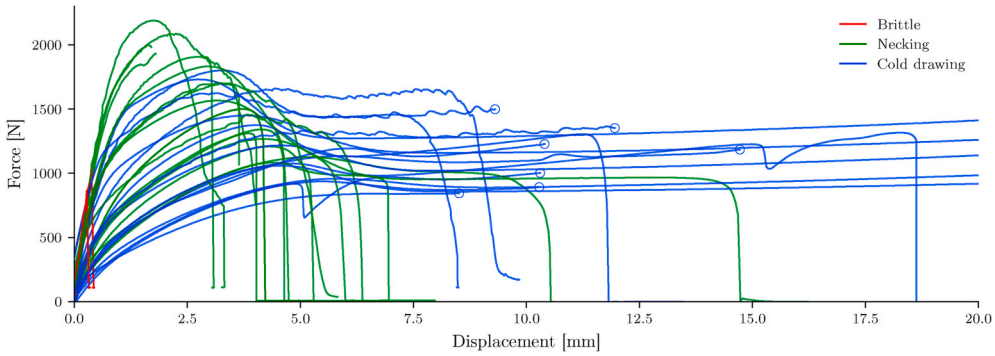

Fig. 6. Force-displacement curves for all tests. The three tensile response regimes are shown in different colours: brittle failure (red lines), failure at necking (green lines) and failure after cold-drawing (blue lines). The circles indicate tests interrupted after the onset of cold-drawing. (For interpretation of the references to colour in this figure legend, the reader is referred to the Web version of this article.)

keeping the variable *b* at its high level.

All computations were performed using the Python™ programming language and the toolkit PANDAS [26].

3. Results and discussion

In the following, the results from the tensile tests are presented and discussed, starting with a qualitative overview on how the shape of the specimen evolves due to necking and strain localization. To corroborate the observations made for the specimen response, the changes in the materials' true stress-strain response are presented and discussed. Thereafter, Section 3.2 presents and discusses the factor analysis of the response parameters introduced in Section 2.4.

3.1. Three response regimes

The tensile response of the specimens spans from brittle to very ductile. During elongation, the tensile specimens normally undergo an initially elastic deformation followed by yielding and associated necking and finally a cold drawing process. Depending on the degradation and loading conditions, however, failure of the specimens was observed at all three stages of deformation. Hence, the specimen responses can be divided into three regimes:

1. Brittle failure with no apparent plasticity.
2. Ductile failure at necking without cold drawing.
3. Ductile failure after cold drawing.

Fig. 5 shows a deformed specimen immediately before failure for the three cases of brittle failure, ductile failure at necking, and ductile failure after cold drawing. Note that the elongation in the latter case is much larger than when the specimen fails during the necking process, translating to significantly larger nominal strain at failure.

The macroscopic response of all specimens is shown in terms of force vs. displacement in Fig. 6. The three regimes are indicated in Fig. 6 by different colours, i.e. the red, green and blue curves correspond respectively to specimens that exhibited brittle behaviour, failed at or shortly after necking, or failed after cold drawing. The tests performed at high rate were all elongated to failure whereas the specimens deformed at low rate were interrupted after the onset of cold drawing to reduce the duration of the tests. In Fig. 6, an interrupted test is indicated by a hollow circle at the end point of the curve.

A brittle response was observed for the two replicate R2 specimens with an initial softener content of 0% and a CIV of 0.7 dL/g deformed with high rate at −10 °C. The combination of low softener contents, low CIV and low temperature represents a state which increases the force level, apparently promoting brittle failure. Both brittle specimens failed in the vicinity of the threads, suggesting that the material was highly sensitive to defects at these conditions.

In order to gain a clearer view of the influence of the five factors introduced in Section 2.1, the force-displacement curves from all 36 tensile tests are shown in Fig. 7, where tests at various temperatures, rates and notch radii are presented in different sub-figures. Thus, the curves in each sub-figure reflect the impact of the plasticizer content and CIV level. According to Fig. 7, most specimens with a CIV of 0.7 dL/g failed at necking, whereas almost all specimens with a CIV of 1.2 dL/g exhibited necking followed by cold drawing. Similar studies [1,4,5] have reported large nominal strains at failure for degraded PA11 with average molecular weights corresponding to a CIV in the order of 1.2 dL/g, suggesting that cold drawing was present also in their tests. It is

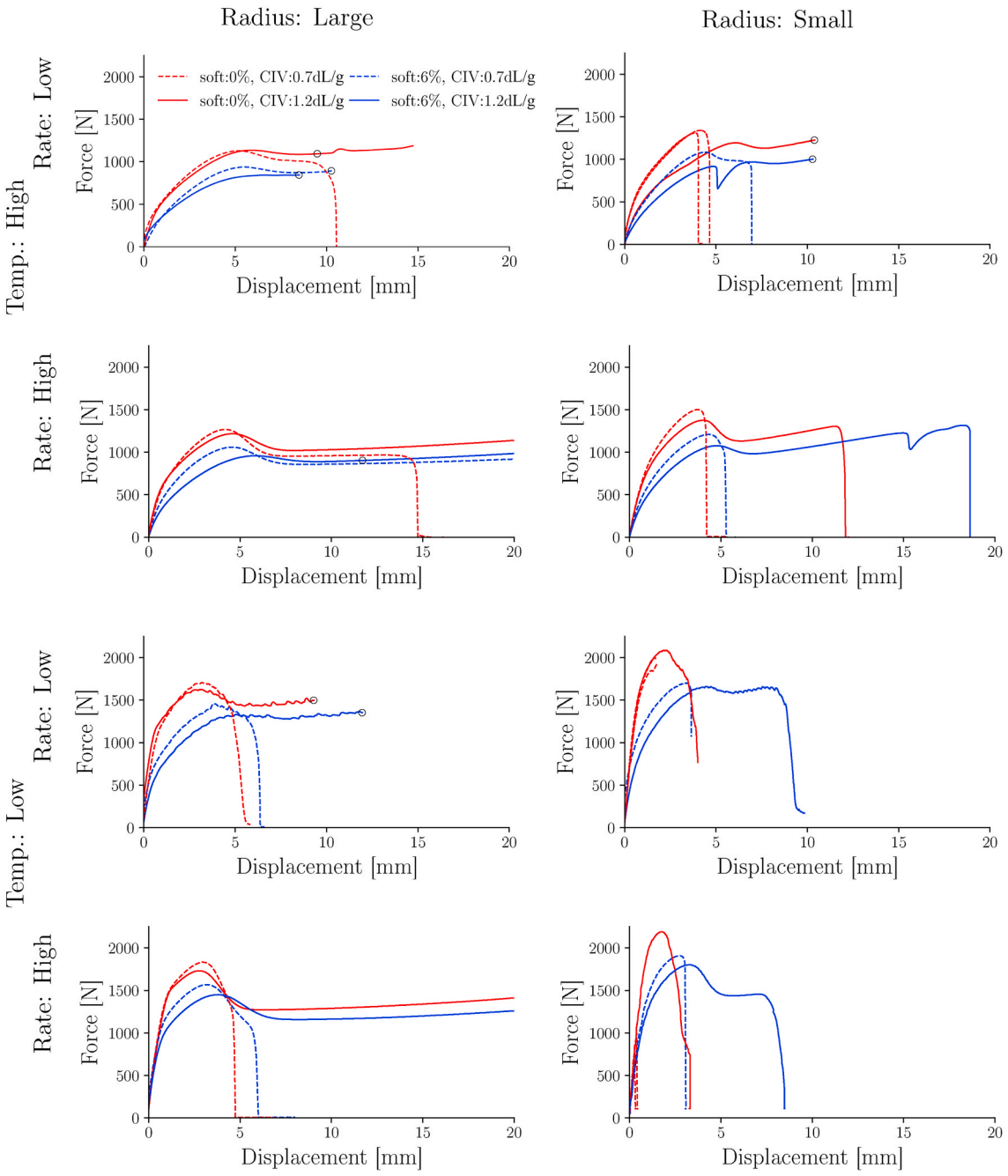

Fig. 7. Force-displacement curves for all test specimens.

here evident that the transition from ductile towards more brittle response in terms of nominal strain at failure could be attributed to the transition between failure after cold drawing and failure at necking.

Fig. 8 shows the true stress-strain curves corresponding to the 36 force-displacement curves in Fig. 7. While it was rather straightforward to distinguish between failure at necking or failure after cold drawing in Figs. 7 and 8 shows that the true strain at failure is high for most specimens independent of failure mode. This observation suggests that the reduced elongation to failure in many of the force-displacements curves in Fig. 7 is due to the absence of cold drawing and not necessarily a reduced failure strain.

Fig. 9 shows the true strain at failure (or interruption of the test) vs. the displacement at failure for all 36 tests. The colour scheme of the figure addresses the three failure modes in a similar fashion as in Fig. 6, while the size of the circles indicates the two different specimens R2 and R20. The open circles are associated with the tests interrupted after the onset of cold drawing. Fig. 9 shows that the true strain at failure for specimens that fail during necking spans from 0.25 to 1.7 despite having similar displacement to failure. When only nominal strains are considered, this observation would not be possible, highlighting the importance of full field strain measurements when the tensile response of materials is assessed. For the specimens that fail during cold-drawing, the true strain at failure is 1.25 or larger in all cases, while the displacement at failure in general is much larger than for the specimens that fail by necking. Fig. 9 suggests that the true strain at failure does not provide sufficient information to conclude on the ductility of a specimen and that the material's ability to cold draw is a feature which is necessary for a highly ductile specimen response.

This observation raises the question of which mechanism governs the material's ability to cold draw and not fail during necking. A possible

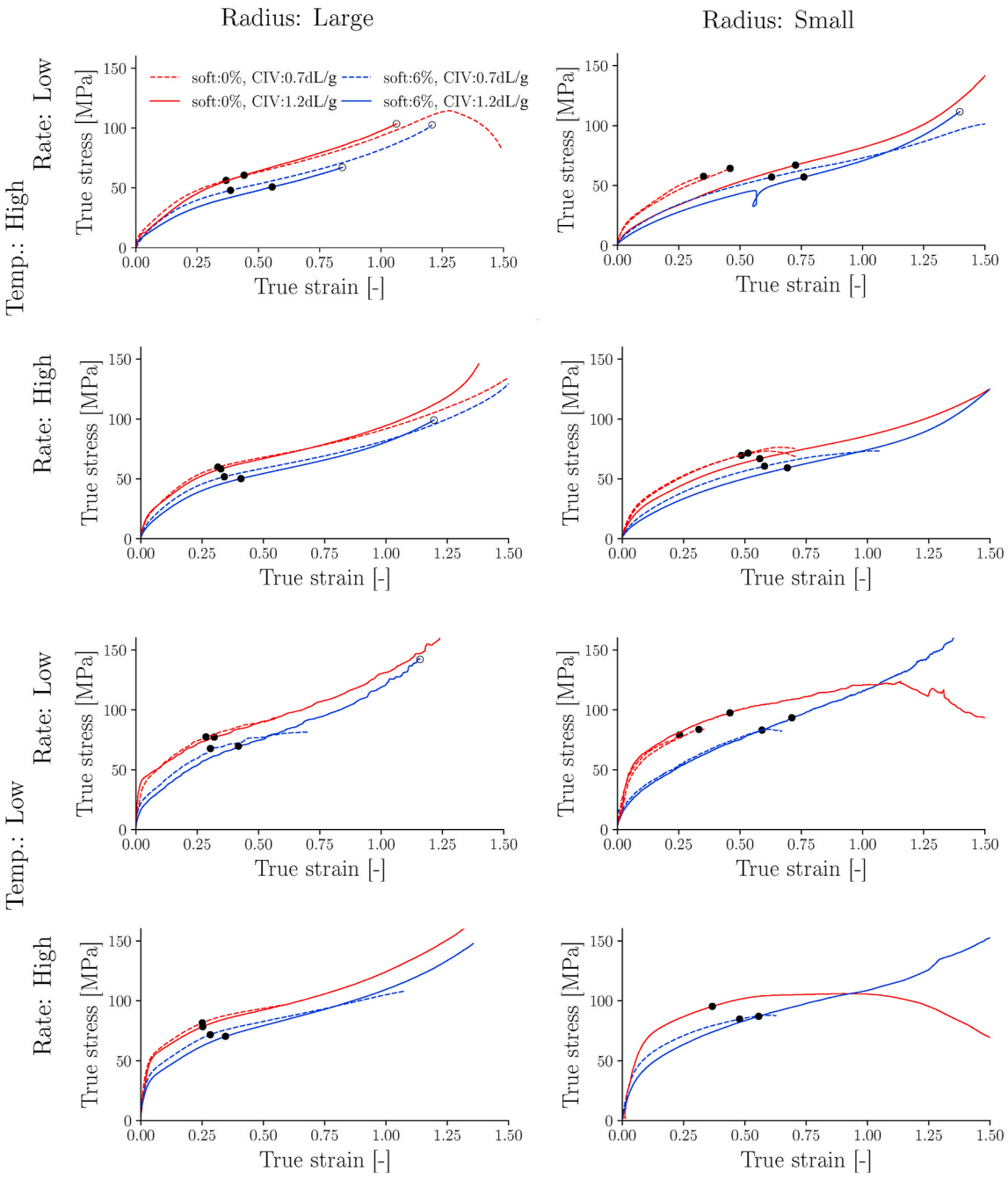

Fig. 8. True stress-strain curves for all test specimens. The point corresponding to peak force is marked with black dots. Tests aborted before failure of the specimen are marked by a hollow circle.

mechanism causing the shift from cold drawing to failure at necking is damage-induced softening. An indication on damage due to void growth is gained by assessing the volumetric strain as calculated by Equation (5) and shown in Figure A1, where it is plotted as function of true strain. The evolution of volumetric strain is very different for the R20 and R2 specimens, where a volumetric strain in the order of 0.3 is reached for all R2 specimens, whereas it is around one order of magnitude lower for the R20 specimens. Numerous studies have reported that stress triaxiality has a strong influence on the degree of cavitation in polymeric materials [7,8,14,27], a finding supported by this study. A non-linear volumetric strain evolution is observed for most R2 specimens, where the rate of change decreases with strain. This behaviour could be caused by blunting of the notch during cold-drawing, which could lower the stress triaxiality within the notch. When semi-crystalline polymers cavitate, voids typically form within the amorphous inter-lamellar phases [28]. As the degradation process reduces the molecular weight, and thereby possibly reduces the load-carrying capacity of the amorphous phase, one could expect that the degraded material is more prone to caviation. However, as large volumetric strains are observed for all specimens with the smallest notch radius, the hypothesis is not directly supported by the findings of this study. Also, previous tensile tests on virgin PA11 with a softener content of 12% showed that the volumetric strains were similar to those observed in this study [29].

3.2. *The influence of loading conditions*

The response parameters selected in Section 2.4 are here presented and discussed. The full test matrix and the values of the response

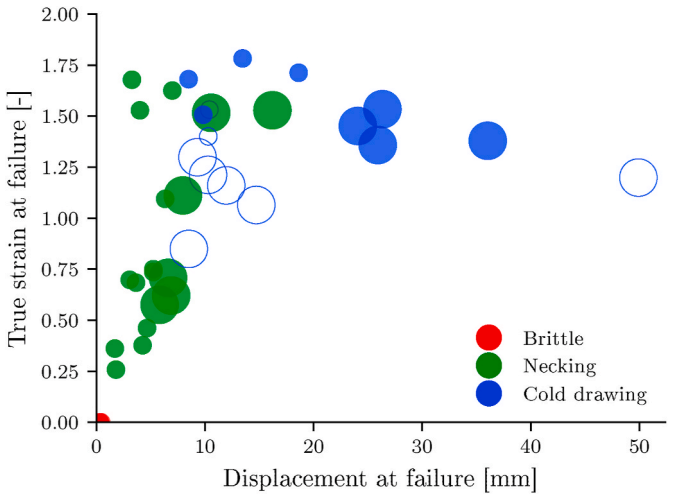

Fig. 9. True strain at failure vs. displacement at failure shown for all tensile specimens. The three failure regimes are shown with different colours, a hollow circle means that the test was aborted before failure, and a large and small circle denote R20 and R2 specimens respectively. (For interpretation of the references to colour in this figure legend, the reader is referred to the Web version of this article.)

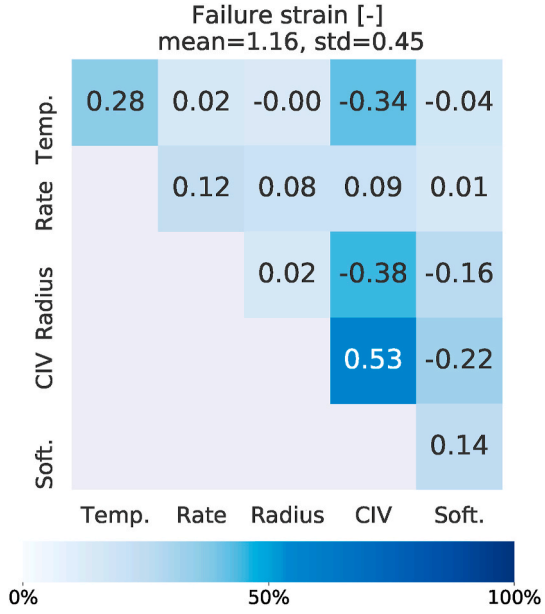

Fig. 10. The main effects and interactions of temperature, strain rate, notch radius, CIV level and softener content on the failure strain. The colours indicate the magnitude of the values relative to the mean value. (For interpretation of the references to colour in this figure legend, the reader is referred to the Web version of this article.)

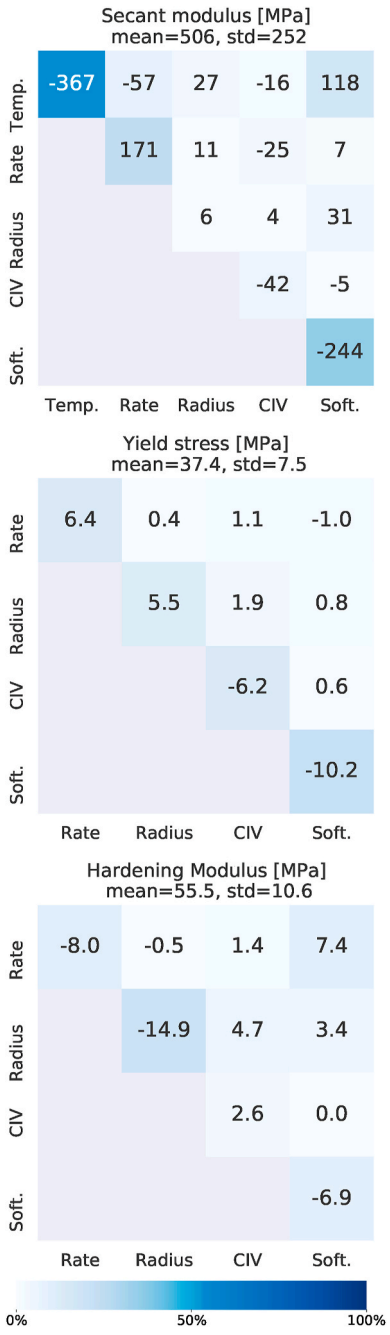

Fig. 11. The main effects and interactions of temperature, strain rate, notch radius, CIV level and softener content on the secant modulus, yield stress and hardening modulus. Note that the effects of hardening modulus and yield stress are only assessed for the specimens deformed at 23 °C. The colours indicate the magnitude of the values relative to the mean value. (For interpretation of the references to colour in this figure legend, the reader is referred to the Web version of this article.)

parameters found from each of the 36 tests are compiled in Table A1. In an attempt to find the reason for the transition from failure after cold drawing to failure at necking, the effects of the variables on the response parameters are assessed.

Fig. 10 shows the calculated main effects and interactions of temperature, strain rate, notch radius, CIV and softener content on the true strain at failure. The diagonal elements of the matrix in Fig. 10 represent the main effects of each factor in the experimental design, whereas the off-diagonal elements represent the interactions. The colours used in Fig. 10 indicate the magnitude of the effects and interactions normalized to the mean value. The model parameter with the largest impact on the failure strain ϵ_f is the CIV where a lower CIV corresponds to a reduced failure strain. According to Table 2, a low CIV corresponds to a higher degree of crystallinity which supports that the degree crystallinity can be used as an indicator on the degree of embrittlement. However, it should here be empasized that the embrittlement is now based on lower local failure strain and not the nominal failure strain, which reduces the influence of necking and cold-drawing. Among the other parameters, temperature is the most important one with respect to the failure strain.

Pronounced interaction effects, both negative, are present between CIV and temperature, and between CIV and notch radius. This means that the CIV level is of greater importance at low temperature and high

triaxiality, which corresponds to the state where two specimens experienced brittle failure. It appears that factors giving a higher stress level promote lower ductility, in particular when the CIV is low. Further, the failure strain ϵ_f is higher at high temperature, possibly related to the lower stress level associated with increased mobility of molecule chains.

Fig. 11 shows the calculated main effects and interactions of temperature, strain rate, notch radius, CIV and softener contents on secant modulus, yield stress and hardening modulus. By inspection of Figs. 8 and 11, it can be observed that the stiffness E_{sec} of the material is highest when the temperature is low, the strain rate is high, or the softener content is low. A higher stiffness at high rate or low temperature is commonly observed for thermoplastics, see e.g. Ref. [6], and is attributed to decreased mobility of the inter-lamellar amorphous phase. However, the influence of temperature is higher when the softener contents is high. When the softener contents is high, the glass transition temperature is anticipated to be around 0 °C, which implies that the high and low temperature is on either side of the glass transition temperature, possibly amplifying the effect of temperature. The magnitude of the effects relative to the mean value indicates that the secant modulus is highly sensitive to all factors except the notch radius and CIV.

The yield stress σ_{20} of the material is highest when the strain rate is high, the notch radius is large, the CIV is low or the softener content is low. A positive correlation between rate and yield stress is commonly observed for rate-sensitive materials. The higher yield stress for large notch radius (i.e., lower stress triaxiality) shows that the material is pressure-sensitive, possibly caused by the dilating nature of the material at high triaxiality, acting as a softening mechanism. The higher yield stress for a low CIV could be explained by increased lamellar thickness caused by chemi-crystallization, cf. the crystallinity measurements of Fig. 2. Previously, Okamba-Diogo et al. [1] and Hocker et al. [2] have addressed the correlation between lamellar thickness and the yield stress of semi-crystalline thermoplastics. It is also observed from Fig. 11 that the yield stress is less sensitive to the model parameters than the secant modulus.

The hardening modulus H does not vary much between the various stress-strain curves in Fig. 8, and the level of degradation does not play a major role for this parameter. Nevertheless, Fig. 11 shows that the hardening modulus is lower when the strain rate is high and the notch radius is large (i.e., low stress triaxiality). Lower hardening modulus at low triaxiality is striking, as the dilating nature of the material at high stress triaxiality is anticipated to act as a softening mechanism, which should lower the hardening modulus. However, this observation could be related to the applied definition of the hardening modulus. The filled circles in Fig. 8, addressing the peak force, suggest that the hardening modulus is calculated during different stages of the deformation process for different specimens. This implies that the strain rate, specimen geometry and stress triaxiality may vary between different specimens, possibly affecting the measured hardening modulus.

As two specimens failed in a brittle manner when deformed at −10 °C, the effects related to the yield stress and hardening modulus are calculated for the samples tested at 23 °C only. It should be noted that self-heating is likely to be present during tensile testing at the high rate. Although not measured in this study, previous experiments on similar specimens but with a softener content of 12% have shown a temperature increase of tens of degrees before failure for a similar strain rate [29]. However, as there is limited dissipation at small plastic deformations, the secant modulus and yield stress are considered to be measured under iso-thermal conditions.

As two repetitions were performed for a minor selection of variable combinations, a statistical assessment of the repeatability is not possible. However, the deviation in mechanical response between the duplicate tests is limited and the observed repeatability is considered to be sufficient for the qualitative assessment performed in this study. During testing, two R2 specimens slipped in the clamps at 15 mm and 5 mm elongation, respectively. As the data used in the analyses were extracted before this elongation, the conclusions from the study are unaffected.

Due to the non-linear visco-plastic response of the material, it is difficult to identify the factors causing the transition between the three regimes of tensile response. Although not observed directly in this study, an abrupt increase in strain hardening is a mechanism that could promote the transition from failure at necking to failure after cold drawing. Such an increase in strain hardening at large strain is commonly reported for polymeric materials, being attributed to the orientation and locking of chains in the amorphous inter-lamellar phase. The amorphous phase is also the region where the chain-scission process is anticipated to be most pronounced [1,4,30]. A possible consequence of the reduced molecular weight in the amorphous phase could be the absence of chain-locking, or a reduced load-carrying capacity when locking is initiated, thereby causing the observed transition to failure during necking.

4. Conclusion

Motivated by the complex loads found in real-world structures, this study demonstrated how temperature, strain rate and notch geometry influence the tensile response of specimens made of chemically degraded PA11. The failure responses were classified into three groups, namely brittle failure, ductile failure during necking and ductile failure after cold-drawing. It was shown that by changing the experimental conditions, a shift in specimen response between these three groups could be obtained. All parameters that increased the stress level within the specimen appeared to promote a more brittle behaviour. Local strain measurements showed that large local strains were present even for specimens that failed during necking, suggesting that the commonly observed reduction in nominal strain at failure could be caused by the presence or absence of cold drawing and not a reduced local strain at failure. This study highlights the importance of carefully evaluating the experimental conditions used when studying the embrittlement of PA11 while showcasing the additional insight gained through full-field strain measurements.

CRediT authorship contribution statement

Sindre Nordmark Olufsen: Conceptualization, Methodology, Software, Formal analysis, Investigation, Visualization, Writing – original draft. **Per Nygård:** Conceptualization, Methodology, Writing – review & editing. **Catarina Ines Teixeira Pais:** Conceptualization, Methodology, Investigation, Writing – original draft. **Giovanni Perillo:** Conceptualization, Methodology, Writing – review & editing. **Odd Sture Hopperstad:** Conceptualization, Methodology, Writing – review & editing, Supervision. **Arild Holm Clausen:** Conceptualization, Methodology, Writing – review & editing, Supervision.

Declaration of competing interest

The authors declare that they have no known competing financial interests or personal relationships that could have appeared to influence the work reported in this paper.

Acknowledgements

The authors gratefully appreciate the financial support from the Research Council of Norway through the Centre for Advanced Structural Analysis, Project No. 237885 (SFI-CASA). We thank Arkema for providing customised material for this study.

Appendix

Table A.1
Test conditions and results for all specimens. The hardening modulus H is set to 0 in tests with failure strain less than 0.4. Further, σ_{20}, H and ϵ_f are disregarded for the two brittle specimens. Repeated tests are highlighted in grey.

Variables					Response parameters					
Temp. [°C]	Strain rate [s^{-1}]	Notch radius [mm]	CIV [dL/g]	Soft. [%]	E_{sec} [MPa]	σ_{20} [MPa]	H [MPa]	u_f [mm]	ε_f [-]	Fail.
-10	0.001	2	0.7	0	855	72.9	0.0	1.80	0.26	Neck.
-10	0.001	2	0.7	0	795	71.3	0.0	1.70	0.36	Neck.
-10	0.001	2	0.7	6	266	48.1	78.1	3.65	0.68	Neck.
-10	0.001	2	1.2	0	890	76.0	63.5	4.01	1.53	Neck.
-10	0.001	2	1.2	6	389	45.9	79.8	9.84	1.51	C.D.
-10	0.001	20	0.7	0	740	68.2	44.3	5.82	0.58	Neck.
-10	0.001	20	0.7	6	416	53.9	49.9	6.60	0.71	Neck.
-10	0.001	20	1.2	0	670	66.5	60.7	9.31	1.30	C.D.
-10	0.001	20	1.2	6	411	48.1	69.7	11.96	1.16	C.D.
-10	0.10	2	0.7	0	988[3]	2.2	0.0	0.32	0.00	Brit.
-10	0.10	2	0.7	0	988[3]	1.8	0.0	0.43	0.00	Brit.
-10	0.10	2	0.7	6	759	66.0	47.7	3.07	0.70	Neck.
-10	0.10	2	1.2	0	898	82.6	46.5	3.27	1.68	Neck.
-10	0.10	2	1.2	6	588	58.3	69.7	8.49	1.68	C.D.
-10	0.10	20	0.7	0	988	76.8	35.5	6.89	0.62	Neck.
-10	0.10	20	0.7	6	642	63.2	43.0	7.97	1.11	Neck.
-10	0.10	20	1.2	0	968	73.6	47.4	24.08	1.45	C.D.
-10	0.10	20	1.2	6	601	56.9	56.0	25.91	1.36	C.D.
23	0.001	2	0.7	0	342	41.1	81.9	4.66	0.46	Neck.
23	0.001	2	0.7	0	387	43.7	81.9[1]	4.25	0.38	Neck.
23	0.001	2	0.7	6	218	29.6	57.4	6.99	1.63	Neck.
23	0.001	2	1.2	0	267	29.5	71.4	10.40	1.53	C.D
23	0.001	2	1.2	6	168	23.8	56.0	10.30	1.40	C.D
23	0.001	20	0.7	0	305	42.8	50.7	10.57	1.52	Neck.
23	0.001	20	0.7	6	303	35.5	45.6	10.28	1.21	C.D
23	0.001	20	1.2	0	311	39.3	62.5	14.72	1.06	C.D
23	0.001	20	1.2	6	193	29.8	50.6	8.51	1.06[2]	C.D
23	0.10	2	0.7	0	512	47.5	55.2	5.24	0.75	Neck.
23	0.10	2	0.7	0	473	46.9	61.3	5.24	0.74	Neck.
23	0.10	2	0.7	6	297	34.3	58.3	6.33	1.09	Neck.
23	0.10	2	1.2	0	403	40.1	60.7	13.46	1.78	C.D
23	0.10	2	1.2	6	241	29.0	59.5	18.63	1.71	C.D
23	0.10	20	0.7	0	473	50.0	39.7	16.21	1.53	Neck.
23	0.10	20	0.7	6	360	41.1	41.8	26.34	1.53	C.D
23	0.10	20	1.2	0	475	47.5	46.4	36.04	1.38	C.D
23	0.10	20	1.2	6	294	35.6	47.4	49.91	1.20	C.D

[1] Set to the value of the duplicate test
[2] This test was aborted prematurely and the strain value is set to that of the corresponding low softener test
[3] The test failed in a brittle manner and the value was set to the one obtained for the corresponding R20 specimen.

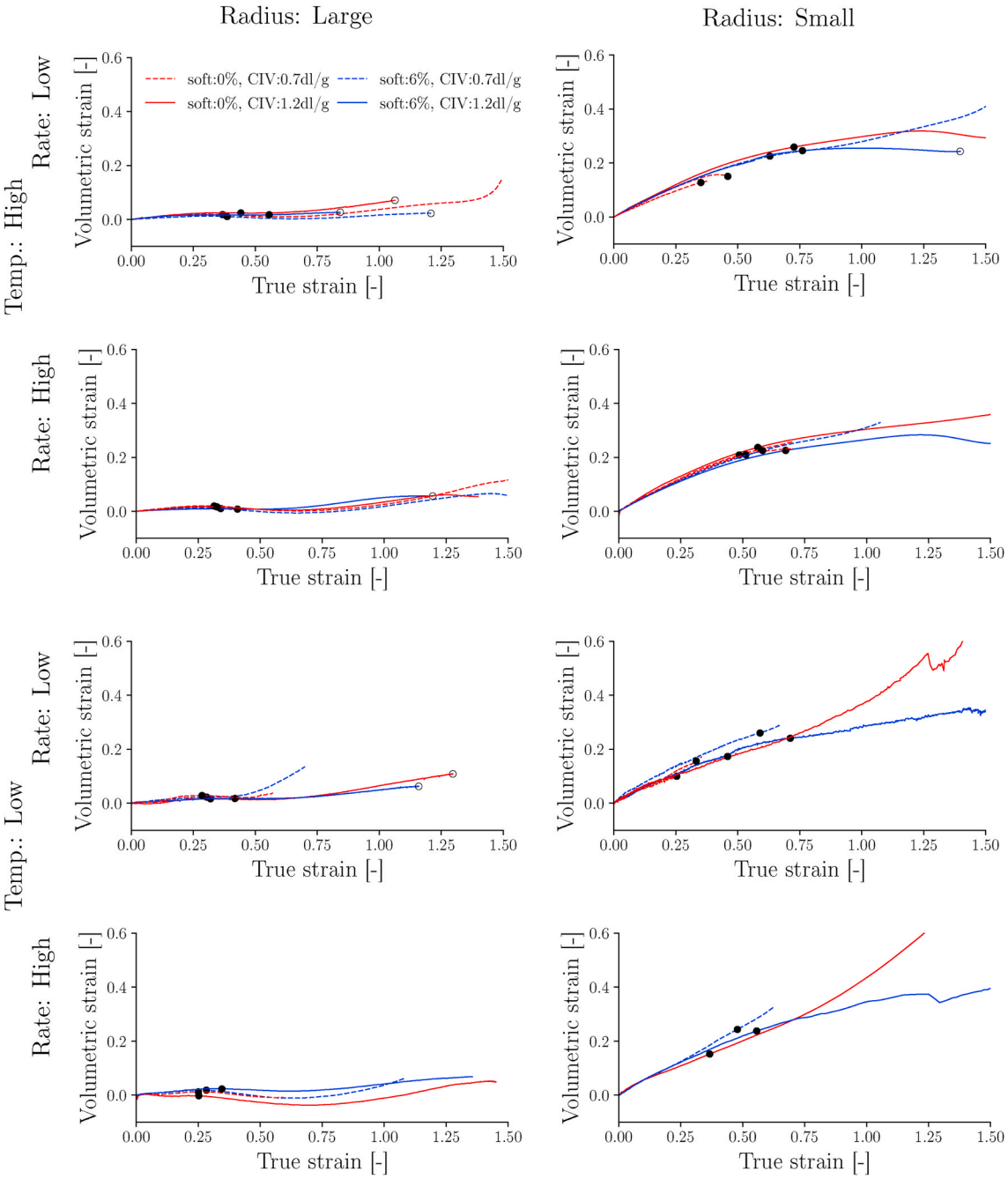

Fig. A.1. Volumetric strain vs. strain curves for all test specimens. The point corresponding to peak force is marked with black dots.

References

[1] O. Okamba-Diogo, E. Richaud, J. Verdu, F. Fernagut, J. Guilment, B. Fayolle, Investigation of polyamide 11 embrittlement during oxidative degradation, Polymer 82 (2016) 49–56.

[2] S.J. Hocker, W.T. Kim, H.C. Schniepp, D.E. Kranbuehl, Polymer crystallinity and the ductile to brittle transition, Polymer 158 (2018) 72–76.

[3] API Technical Report 17TR2, the Ageing of PA-11 in Flexible Pipes, first ed., 2003.

[4] S.J. Hocker, W.T. Kim, H.C. Schniepp, D.E. Kranbuehl, Polymer crystallinity and the ductile to brittle transition, Polymer 158 (2018) 72–76.

[5] B. Fayolle, E. Richaud, X. Colin, J. Verdu, Review: degradation-induced embrittlement in semi-crystalline polymers having their amorphous phase in rubbery state, J. Mater. Sci. 43 (2008) 6999–7012.

[6] J. Johnsen, F. Grytten, O.S. Hopperstad, A.H. Clausen, Influence of strain rate and temperature on the mechanical behaviour of rubber-modified polypropylene and cross-linked polyethylene, Mech. Mater. 114 (2017) 40–56.

[7] S.N. Olufsen, A.H. Clausen, O.S. Hopperstad, Influence of stress triaxiality and strain rate on stress-strain behaviour and dilation of mineral-filled PVC, Polym. Test. 75 (2019) 350–357.

[8] A.S. Ognedal, A.H. Clausen, A. Dahlen, O.S. Hopperstad, Behavior of PVC and HDPE under highly triaxial stress states: an experimental and numerical study, Mech. Mater. 72 (2014) 94–108.

[9] J.A. van Dommelen, M. Poluektov, A. Sedighiamiri, L.E. Govaert, Micromechanics of semicrystalline polymers: towards quantitative predictions, Mech. Res. Commun. 80 (2017) 4–9.

[10] Z. Bartczak, A. Galeski, Plasticity of semicrystalline polymers, Macromol. Symp. 294 (2010) 67–90.

[11] Z. Bartczak, Deformation of semicrystalline polymers – the contribution of crystalline and amorphous phases, Polimery 62 (2017) 787–799.

[12] M. Walczak, The Role of the Amorphous Phase in Semi-crystalline Polymers, Ph.D. thesis, 2013.

[13] A. Rozanski, A. Galeski, Plastic yielding of semicrystalline polymers affected by amorphous phase, Int. J. Plast. 41 (2013) 14–29.

[14] S.N. Olufsen, A.H. Clausen, D.W. Breiby, O.S. Hopperstad, X-ray computed tomography investigation of dilation of mineral-filled PVC under monotonic loading, Mech. Mater. 142 (2020) 103296.
[15] L. Laiarinandrasana, O. Klinkova, F. Nguyen, H. Proudhon, T.F. Morgeneyer, W. Ludwig, Three dimensional quantification of anisotropic void evolution in deformed semi-crystalline polyamide 6, Int. J. Plast. 83 (2016) 19–36.
[16] P.A. Poulet, G. Hochstetter, A. King, H. Proudhon, S. Joannès, L. Laiarinandrasana, Observations by in-situ X-ray synchrotron computed tomography of the microstructural evolution of semi-crystalline Polyamide 11 during deformation, Polym. Test. 56 (2016) 245–260.
[17] L. Laiarinandrasana, N. Selles, O. Klinkova, T.F. Morgeneyer, H. Proudhon, L. Helfen, Structural versus microstructural evolution of semi-crystalline polymers during necking under tension: influence of the skin-core effects, the relative humidity and the strain rate, Polym. Test. 55 (2016) 297–309.
[18] Y. Kong, J.N. Hay, The measurement of the crystallinity of polymers by DSC, Polymer 43 (2002) 3873–3878.
[19] J. Johnsen, F. Grytten, O.S. Hopperstad, A.H. Clausen, Experimental set-up for determination of the large-strain tensile behaviour of polymers at low temperatures, Polym. Test. 53 (2016) 305–313.
[20] A. Ilseng, B.H. Skallerud, A.H. Clausen, Volume growth during uniaxial tension of particle-filled elastomers at various temperatures – experiments and modelling, J. Mech. Phys. Solid. 107 (2017) 33–48.
[21] A. Ilseng, B.H. Skallerud, A.H. Clausen, Tension behaviour of HNBR and FKM elastomers for a wide range of temperatures, Polym. Test. 49 (2016) 128–136.
[22] M.A. Sutton, J.-J. Orteu, H.W. Schreier, Image correlation for shape, Motion and Deformation Measurements 53 (2009).
[23] E. Fagerholt, Field Measurements in Mechanical Testing Using Close-Range Photogrammetry and Digital Image Analysis, Ph.D. thesis, NTNU, 2012.
[24] S.N. Olufsen, M.E. Andersen, E. Fagerholt, μDIC: an open-source toolkit for digital image correlation, Software 11 (2020) 100391.
[25] D.C. Montgomery, Design and Analysis of Experiments Eighth Edition 2 (2012).
[26] W. McKinney, Data structures for statistical computing in Python, in: Proceedings of the 9th Python in Science Conference, pp. 51–56.
[27] G. Boisot, L. Laiarinandrasana, J. Besson, C. Fond, G. Hochstetter, Experimental investigations and modeling of volume change induced by void growth in polyamide 11, Int. J. Solid Struct. 48 (2011) 2642–2654.
[28] A. Pawlak, A. Galeski, A. Rozanski, Cavitation during deformation of semicrystalline polymers, Prog. Polym. Sci. 39 (2013) 921–958.
[29] H. Dahle, O.K. Rønning, Thermomechanical Response of Virgin and Degraded, 2019, p. PA11.
[30] S. Hocker, A.K. Rhudy, G. Ginsburg, D.E. Kranbuehl, Polyamide hydrolysis accelerated by small weak organic acids, Polymer 55 (2014) 5057–5064.